A&A 392, 161–167 (2002)
DOI: 10.1051/0004-6361:20020923

Astronomy & Astrophysics

New measurements of orbital period change in Cygnus X-3

N. S. Singh[1], S. Naik[2], B. Paul[2], P. C. Agrawal[2], A. R. Rao[2], and K. Y. Singh[1]

[1] Dept. of Physics, Manipur University, Canchipur, Imphal 795003 Manipur, India
[2] Tata Institute of Fundamental Research, Homi Bhabha Road, Mumbai 400005, India

Received 25 January 2002 / Accepted 6 June 2002

Abstract. The nonlinear nature of the binary ephemeris of Cygnus X-3 indicates either a change in the orbital period or an apsidal motion of the orbit. We have made extended observations of Cygnus X-3 with the Pointed Proportional Counters (PPCs) of the Indian X-ray Astronomy Experiment (IXAE) during 1999 July 3−13 and October 11−14. Using the data from these observations and the archival data from ROSAT, ASCA, BeppoSAX and RXTE, we have extended the database for this source. Adding these new arrival time measurements to the published results, we make a comparison between the various possibilities, (a) orbital decay due to mass loss from the system, (b) mass transfer between the stars, and (c) apsidal motion of the orbit due to gravitational interaction between the two components. The orbital decay due to mass loss from the companion star seems to be the most probable scenario.

Key words. stars: binaries: close – stars: individual: Cygnus X-3 – stars: Wolf-Rayet – X-rays: stars

1. Introduction

The nature of the compact object in the bright X-ray binary Cygnus X-3 is a subject of much debate. In spite of being one of the most frequently observed X-ray sources, the presence of an X-ray pulsar, a black hole, or a low magnetic field neutron star has not yet been established. There is also uncertainty about the mass and type of the companion star. An interesting way to probe this system is to investigate the arrival time history of the 4.8 hr orbital modulation in the X-ray light curve.

The unusual X-ray binary Cygnus X-3 is located in the plane of our galaxy at a distance of >11.6 kpc (Dickey 1983). Because of the high luminosity of the source in X-ray, infrared and radio bands, it has been observed on many occasions at these wavelengths. Strong optical extinction in the direction of the source prevents optical observations. The mass of the companion star has been determined by many different means and it is found to be in the range of a fraction of solar mass to a few solar mass (Van den Heuvel & De Loore 1973; Tavani et al. 1989; van Kerkwijk et al. 1992). Parsignault et al. (1976) discovered a periodicity of 4.8 hr in the X-ray flux with nearly sinusoidal variation, which is believed to be due to the orbital motion. The variation in the sinusoidal shape of the light curve from cycle to cycle is reported by van der Klis & Bonnet-Bidaud (1981). They showed that the shape of the average light curve formed from successive cycles is quasi-sinusoidal with a slow rise and fast fall. Several models have been proposed to explain the deep and near-sinusoidal modulation of the X-ray intensity of Cygnus X-3 with the orbital period (Ghosh et al. 1981). Material in the form of a large shell around the binary system can produce the X-ray modulation by scattering, absorbing, and re-emitting the X-rays from the compact object, if the X-ray emission is only from the non-shadowed part of the shell. White & Holt (1982) proposed the accretion disk corona (ADC) model to explain the modulation in the X-ray light curve of the source. According to this model, the X-ray source is covered by an optically thick corona with a radius of about 10^9 cm, an optical depth of about 10 and a temperature of about 2 keV. Another model that tries to explain the orbital modulation is stellar wind model (Willingale et al. 1985; Kitamoto et al. 1987). This model assumes a strong and highly ionized stellar wind from the companion star with an optical depth of about 1 and a radius of about 10^{11} cm and the temperature of the wind is model-dependent.

Evolution of the orbit of Cygnus X-3 is studied by measuring the arrival times of the minima in each orbital motion. The ephemeris of 4.8 hr modulation in the X-ray light curve of the source has been studied by many authors (Leach et al. 1975; Mason & Sanford 1979; Parsignault et al. 1976; Lamb et al. 1979; Elsner et al. 1980; van der Klis & Bonnet-Bidaud 1981, 1989; Kitamoto et al. 1987). The time derivative of the orbital modulation period ($\dot{P}$) and second derivative ($\ddot{P}$) have been measured as $\sim 10^{-9}$ s s^{-1} and $\sim -10^{-11}$ yr (van der Klis & Bonnet-Bidaud 1981, 1989; Kitamoto et al. 1987). The unusually large value of $\dot{P}/P$ ($= 2.2 \times 10^{-6}$ yr^{-1}), which if linked to the binary evolution of the system, is similar to several short-period bright LMXBs such as X1822−371 with $\dot{P}/P \sim 3.4 \times 10^{-7}$ yr^{-1} and has orbital period of 5.57 hr (Hellier et al. 1990; Parmar et al. 2000) or EX00748−767 with $\dot{P}/P \sim 2 \times 10^{-7}$ yr^{-1} and

Send offprint requests to: S. Naik, e-mail: sachi@tifr.res.in

an orbital period of 3.82 hr (Parmar et al. 1991). This value of $\dot{P}$ can be interpreted as due to the mass transfer from the optical companion to the compact object. Using the measured period derivative of Cygnus X−3, Kitamoto et al. (1987) determined the rate of mass loss from the binary companion as about $10^{-6}\ M_{\odot}\ \mathrm{yr}^{-1}$. Tavani et al. (1989) tried to explain the observed high value of $\dot{P}/P$ in Cygnus X-3 and the required mass transfer rate close to $\sim 1.58 \times 10^{-8}\ M_{\odot}\ \mathrm{yr}^{-1}$. They claimed that the companion is a degenerate star with solar composition and in the mass range of $0.01 \leq m \leq 0.03\ M_{\odot}$ which under-fills its Roche lobe. The X-ray illumination from the primary compact object produces the evaporative wind from such a low-mass degenerate companion. However, from infrared observations, van Kerkwijk et al. (1992) discovered that the binary companion of Cygnus X-3 has the spectrum of a Wolf-Rayet star and predicted the mass of the companion as $\sim 10\ M_{\odot}$ which suggests that Cygnus X-3 is a high mass X-ray binary. Recent observations by Fender et al. (1999) confirm the nature of the companion as an early-type WN Wolf-Rayet star.

We have measured the available arrival time of the minimum value of the light curve from two observation of Cygnus X-3 with PPCs of IXAE in 1999 and several sources of archival data. By combing these new measurements with the previously published results, we are able to determine the rate of change of orbital period with greater accuracy.

2. Observations and archival data

2.1. PPC observations

The X-ray observations of Cygnus X-3 were carried out twice on 1999 July 3−13 and 1999 October 11−14 with the 1 s time-integration mode with the PPCs of the IXAE on board the Indian satellite IRS-P3. The IXAE includes three co-aligned and identical, multi-wire, multi-layer proportional counters with a total effective area of 1200 cm^2 covering 2 to 18 keV energy range with an average detection efficiency of about 60% in 3−7 keV energy range. Each PPC is equipped with a honeycomb type collimator having a field of view of $2.^{\circ}3 \times 2.^{\circ}3$ and has an overall energy resolution of about 22% at 6 keV (Agrawal et al. 1998; Rao et al. 1998). The IRS-P3 satellite is in a circular orbit at an altitude of 830 km and inclination of 98°. Pointing towards any particular source is done by using a star tracker with an accuracy of $\leq 0.^{\circ}1$. The useful observation time is limited to the latitude range typically from 30 °S to 50 °N to avoid the rise in charged particle background at high latitudes. The South Atlantic Anomaly (SAA) region restricts the observation to 5 of the 14 orbits per day. As the detectors are co-aligned, simultaneous background observation is not possible. The background counts are measured after the observation of a source by pointing the PPCs to a source-free region in the sky, close to the target source. The total useful exposure time to the X-ray source during the two observations is 31 245 s. The PPC light curves did not show strong intensity variations on the time scale of a few seconds to a few hundred seconds.

2.2. Archival data

We have also analyzed archival data from several satellites. From the ROSAT mission, we have analyzed HRI data with two different observation IDs. The durations of these two observations are *inter-wined*, but the overall count rate is different because in one of the observations, the source was near the edge of the field of view where effective area is small. RXTE/PCA observations of the source in 2−60 keV energy range, combined data from GIS detectors (GIS2 and GIS3) and SIS detectors (SISO and SIS1) of the ASCA satellite and data from MECS detectors of BeppoSAX observations were used to determine more arrival time information of Cygnus X−3. We have analyzed the RXTE/ASM dwell data in the energy range of 2−12 keV for the entire period of observation starting from January 1996 to August 30 2001. The details of the observations of the source with different satellites are given in Table 1 along with the useful exposure period.

Table 1. Archival data used for the determination of the arrival time of the minima of the binary modulation.

Satellite	Date of observation	Exposure (in seconds)	Detector
ASCA	1994 29/5 − 30/5	21 468	GIS
ASCA	1994 29/5 − 30/5	17 527	SIS
ROSAT	1995 20/4 − 22/4	72 709	HRI
ROSAT	1995 21/4 − 23/4	51 670	HRI
BeppoSAX	1996 22/9 − 24/9	51 626	MECS
BeppoSAX	1996 10/10	26 167	MECS
BeppoSAX	1996 29/10	13 664	MECS
BeppoSAX	1997 19/9 − 20/9	25 802	MECS
RXTE	1996 24/8 − 30/8	86 450	PCA
RXTE	1997 16/2 − 22/2	59 465	PCA
RXTE	1997 05/6 − 26/9	64 693	PCA
RXTE	1998 16/5 − 21/5	34 723	PCA
RXTE	1996 04/1 − 2001 30/8		ASM

3. Data analysis and results

3.1. Arrival time determination

The data used for the analysis were corrected to the solar system barycenter. To avoid cycle to cycle variation in the light curve, we have created the time-averaged orbital modulation profile by folding the source light curves with a period of 17 253 s (Elsner et al. 1980). In all cases, the shape of the folded light curves is somewhat similar to the shape of the template function which is the long-term average shape of the light curve obtained with the Copernicus satellite (Mason et al. 1976).

To determine the arrival times of the minimum of the folded light curves, we have used the normalized template data of X-ray ephemeris of Cygnus X-3 (van der Klis et al. 1989). The folded data were cross-correlated with the standard template function as described by van der Klis et al. (1989) to get the phase difference in the minima of the template and the

Table 2. Observations used to determine the ephemeris of Cygnus X-3 (new record).

Observation Period (MJD)	Satellite (detector)	Number of Orbits (p = 17253 s)	Arrival time (2 440 000 JD+) (day)	Error in arrival time (day)
49501.91–49502.84	ASCA (GIS)	42 832	9502.8736	0.0021
49501.91–49502.84	ASCA (SIS)	42 832	9502.8736	0.0028
49827.99–49829.44	ROSAT (PSPC)	44 466	9829.1748	0.0020
49828.59–49830.56	ROSAT (PSPC)	44 470	9829.9766	0.0021
50086.32–50185.98	RXTE (ASM)	46 006	10136.6934	0.0020
50186.06–50285.99	RXTE (ASM)	46 506	10236.5381	0.0020
50319.46–50325.83	RXTE (PCA)	46 940	10323.2031	0.0024
50348.92–50350.18	BeppoSAX (MECS1)	47 074	10349.9609	0.0020
50385.00–50385.52	BeppoSAX (MECS)	47 253	10385.7090	0.0025
50386.31–50485.96	RXTE (ASM)	47 508	10436.6299	0.0020
50495.02–50501.12	RXTE (PCA)	47 818	10498.5391	0.0047
50486.02–50585.87	RXTE (ASM)	48 008	10536.4727	0.0020
50586.16–50685.95	RXTE (ASM)	48 509	10636.5234	0.0020
50604.75–50717.50	RXTE (PCA)	48 635	10661.6787	0.0021
50710.65–50711.26	BeppoSAX (MECS2)	48 884	10711.4014	0.0020
50731.36–50731.90	BeppoSAX (MECS2)	48 988	10732.1738	0.0021
50686.01–50785.73	RXTE (ASM)	49 009	10736.3643	0.0020
50786.51–50883.86	RXTE (ASM)	49 506	10835.6104	0.0021
50886.79–50985.63	RXTE (ASM)	50 012	10936.6533	0.0020
50949.63–50954.98	RXTE (PCA)	50 093	10952.8203	0.0035
50986.41–51085.89	RXTE (ASM)	50 513	11036.6934	0.0020
51086.09–51185.95	RXTE (ASM)	51 013	11136.5381	0.0047
51186.22–51285.96	RXTE (ASM)	51 514	11236.5830	0.0029
51286.03–51385.62	RXTE (ASM)	52 013	11336.2324	0.0021
51361.49–51371.77	IXAE (PPC)	52 168	11367.1836	0.0021
51404.44–51404.64	RXTE (PCA)	52 358	11405.1309	0.0022
51386.16–51485.96	RXTE (ASM)	52 515	11436.4844	0.0023
51461.72–51464.79	IXAE (PPC)	52 651	11463.6338	0.0024
51549.73–51649.73	RXTE (ASM)	53 334	11600.028320	0.0020
51649.90–51749.80	RXTE (ASM)	53 836	11700.274410	0.0020
51750.06–51850.02	RXTE (ASM)	54 338	11800.516600	0.0020
51850.08–51948.81	RXTE (ASM)	54 836	11899.958010	0.0020
51951.46–52051.45	RXTE (ASM)	55 347	12002.000980	0.0020
52051.58–52151.53	RXTE (ASM)	55 848	12102.048830	0.0020

data which give the measure of the arrival time of the minima. In addition to the statistical variations, Cygnus X-3 often shows some short-term intensity variations superposed on the orbital modulation. We have multiplied the statistical error estimates of each folded light curve by some constant factors to make them fit to the template with a reduced χ^2 of 1.0. The arrival time errors were estimated from the uncertainties in determining the center of the Gaussian function of the cross-correlated data. The short-term occasional intensity variations also cause some random fluctuations in the arrival time determinations. Following earlier works (Kitamoto et al. 1995), we have quadratically added 0.002 d to the arrival uncertainties to make them compatible with the previous reported measurements.

This analysis yielded two new arrival points from PPC observations (Singh et al. 2001), two points from ASCA, two points from ROSAT, five points from RXTE/PCA, and four points from BeppoSAX observations. We divided the RXTE/ASM light curve into 19 segments of durations of 100 days as given in Table 2, and determined the arrival times

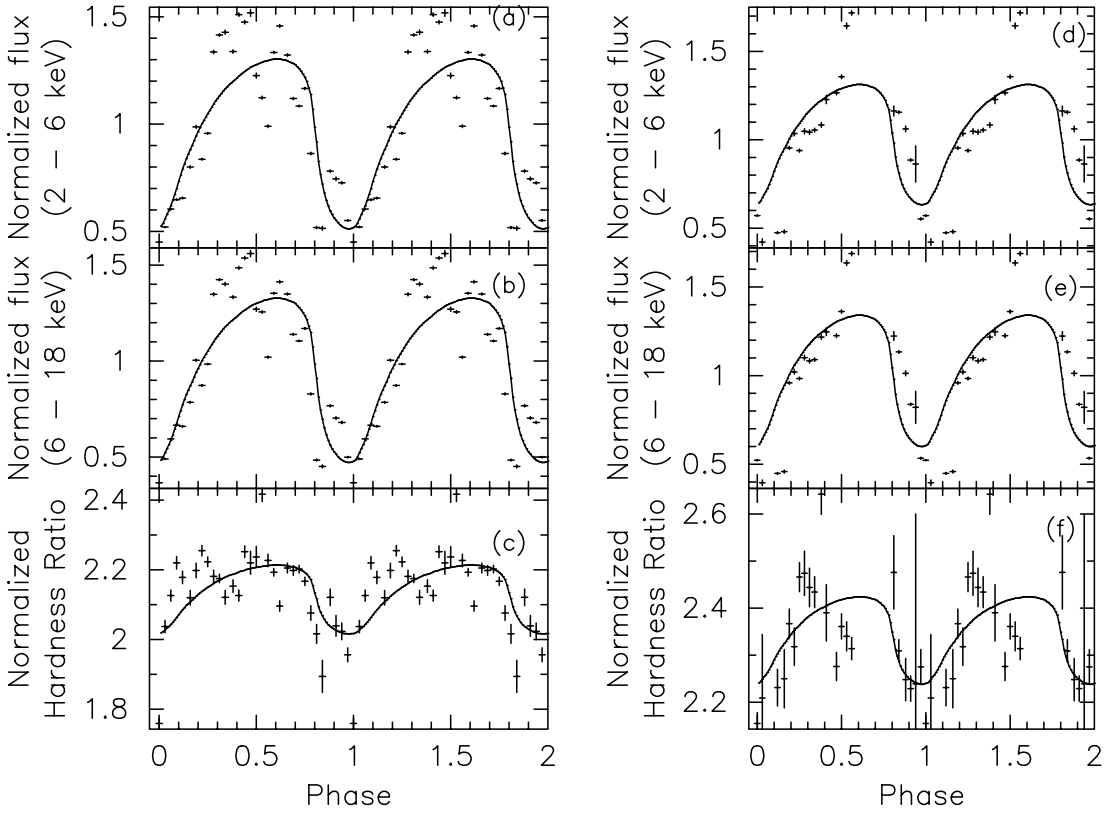

Fig. 1. Folded light curves in the 2−18 keV and 6−18 keV energy ranges are shown in panels **a)** and **b)** (for 1999, July 3−13 PPC observations) and panels **d)** and **e)** (for 1999, October 11−14 PPC observations) on a normalized scale with the template data (described in text) which is indicated by lines. The panels **c)** and **f)** show the folded hardness ratios (ratio of the count rate in 6−18 keV energy range to the count rate in 2−6 keV energy range for 1999, July and October observations respectively).

from each data segment. The information regarding the new arrival times are given in Table 1 along with the observation periods of the source with different instruments on different satellites and the orbit number. In accordance with earlier work (Leach et al. 1975), we have assigned the orbit number of the source as 0 at JD 2440949.9201. The orbit numbers for later observations were calculated by using the 4.8 hour orbital period of the source. The significant addition of a number of new arrival points to the old data improved the numerical values of the period derivative and the double derivative.

The orbital modulation of the light curves obtained from the observations of the source with different instruments are shown in different figures along with the normalized template. Panels (a) and (d) of Fig. 1 show the folded light curves in the 2−18 keV energy range along with the normalized template for the July 3−13 1999 and October 11−14 1999 PPC observations of the source respectively. In Fig. 2, we have shown the orbital modulation of the light curves along with the normalized template for two data segments of the RXTE/ASM for different energy bands. From these figures, it is observed that the shape of the orbital modulated light curves of Cygnus X-3, obtained from various observations, is similar to the shape of the normalized template.

3.2. Orbital evolution of the binary system

Figure 3 (top panel) reports the new measurements of the arrival time of the minima in the orbital modulation of the X-ray light curves of Cygnus X-3 together with those of all the previously published values (Kitamoto et al. 1987; van der Klis & Bonnet-Bidaud 1989). We have tried to fit the arrival time data with different polynomial functions. The residuals of the various polynomial fits performed on these data are also shown in other panels of the figure. The second panel of Fig. 3 shows the residual of the linear fit to the arrival data whereas the third, fourth, and fifth panels of Fig. 3 show the residuals of the quadratic, cubic, and sinusoidal fit to the arrival time data respectively.

The results of the various polynomial fits performed on the complete set of arrival time data are listed in Table 3. The arrival times of the orbital modulations clearly deviate from a linear relationship with the orbit numbers. Addition of a quadratic term fits the data much better with a reduced χ^2 of 3.08 (113 degrees of freedom). From the quadratic fit, the value of the period derivative is derived to be $\dot{P} = 5.76333 \times 10^{-10}$ i.e, an evolution time scale of $\dot{P}/P = 1.05419 \times 10^{-6}$ yr^{-1}. These values are similar to what was obtained with the data prior to 1993 (Kitamoto et al. 1995). A cubic model for the arrival time fits the data slightly better with reduced χ^2 of 2.96 (112 degrees of freedom). However, the rate of change of $\dot{P}$ is found to

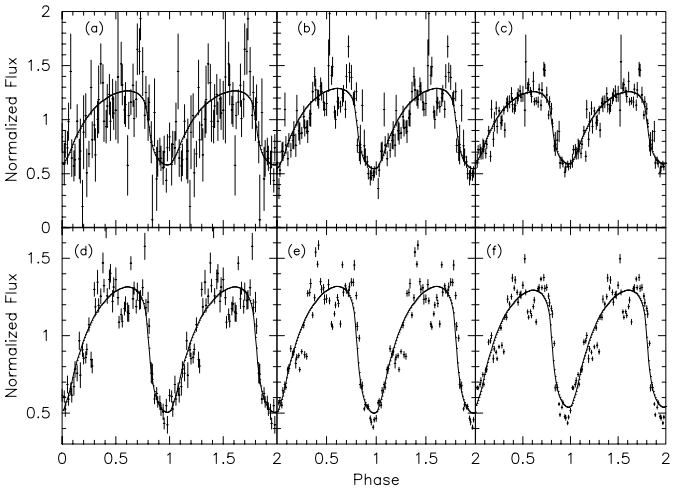

Fig. 2. Normalized folded light curves of the source obtained from the RXTE/ASM data for different energy ranges and at different time. Upper panels (panels **a)–c)**) show the folded light curves in the energy ranges 1.3−3.0 keV, 3.0−5.0 keV, and 5.0–12.1 keV for the data in the time range JD 2450086.8222–2450186.4878 whereas the lower panels (panels **d)–f)**) show the folded light curves in the energy ranges 1.3−3.0 keV, 3.0−5.0 keV, and 5.0–12.1 keV for the data in the time range JD 2450887.2862–JD 2450986.1345 respectively.

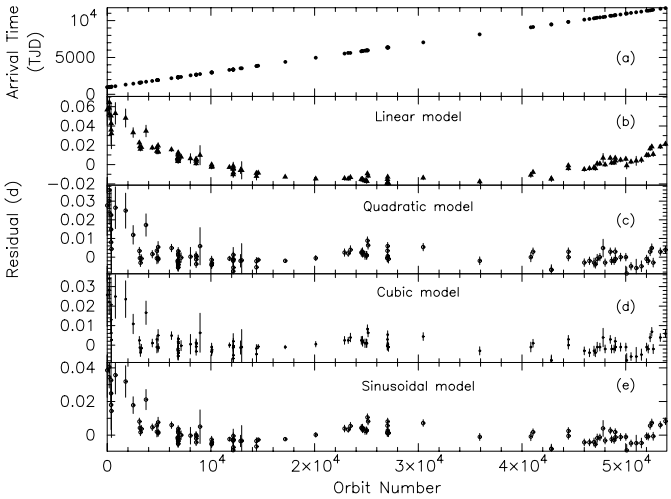

Fig. 3. The arrival time history for the source Cygnus X-3 (top panel). The data points beyond orbit number 42 830 are obtained from the present work. Arrival time residuals of the orbital modulation of the source with respect to the best-fit linear, quadratic, cubic and a linear and sinusoidal models to the data are shown in different panels.

be much smaller compared to that obtained by Kitamoto et al. (1995), $\ddot{P} = -1.34008 \times 10^{-11}$ yr^{-1}. The curved feature of the residual of the linear fit to the data prompted us to fit with a model consisting of linear and sinusoidal terms as model components. Although the reduced χ^2 for this fitting is comparable to the reduced χ^2 for cubic model, the amplitude of sinusoidal component is non-physical because, according to the method described by Batten (1973), it requires the eccentricity of the binary system to be $\gg$1. In the linear plus sinusoidal model, a reduced χ^2 of 3.5 (d.o.f. 112) was obtained by restricting the amplitude of the sinusoidal component within a physical limit so that $e \leq 1$. However, if a precessing eccentric orbit is the reason for the non-linear nature of the arrival times, a change in the shape of the orbital modulation of the light curve is expected, which has not been observed in the last ∼30 years. Based on this argument, apsidal motion seems not to be an appropriate description of the arrival time data.

4. Spectral variations with orbital phases in Cygnus X-3

To investigate the spectral variations of the source during different orbital phases, we have analyzed the hardness ratios from the PPC observations with IXAE on July 3−13 1999 and October 11−14 1999 and the RXTE/ASM data since the beginning of the observation. From the calibration of the PPCs using Crab, it is found that the spectral data from PPC−3 is more reliable. Hence to obtain the hardness ratio (ratio of the count rate in the 6−18 keV energy range to the count rate in 2−6 keV energy range), we have used the data from PPC−3. To study the spectral behavior of the source at different orbital phases, we have created the time averaged profile by folding the light curves and the hardness ratio data with a period of 17 253 s. We have plotted, in Fig. 1, the orbital modulated light curves in the 2−18 keV and 6−18 keV energy ranges and the hardness ratios for the 1999, July and October observations of the source.

The folded RXTE/ASM light curves in the 3−5 keV and 5−12.1 keV energy bands plotted on a normalized scale with the template data and the corresponding hardness ratio for two different epochs (low and high states) are shown in Fig. 2. From the PPC observations (Fig. 1) and the RXTE/ASM observations (Fig. 4), a strong binary phase dependence of the spectrum is noticed.

5. Discussion

The nature of the compact object in the binary system of Cygnus X-3 is not yet clearly understood. There are various arguments in the literature supporting the compact object as a massive black hole whereas some authors believe the primary companion is a neutron star. Schmutz et al. (1996) suggested that the observed time variations in the profile of infrared emission lines from the binary system are due to the orbital motion of the companion which is a Wolf-Rayet star. They derived the mass function for Cygnus X-3 as 2.3 $M_\odot$. They obtained a range of 7−40 $M_\odot$ as the mass of the compact object with a most likely value of 17 $M_\odot$ and suggested that the binary system Cygnus X-3 is composed of a black hole (BH) and a Wolf-Rayet (WR) system. Several models have also been proposed to explain the lengthening of the orbital period (Bonnet-Bidaud & Chardin 1988). Conservative mass transfer from the companion star cannot explain the observations. This is due to the fact that the mass accretion rate needed to produce the amount of energy emitted in X-rays and the observed orbital period change rate requires a very low mass companion ∼0.02 $M_\odot$, which will under-fill its Roche lobe to continue mass transfer. A low mass companion star with a moderate non-conservative mass loss rate, however, can explain the period change rate, if the mass loss is due to X-ray heating of the

Table 3. Statistics of different fitting models to the data of arrival time.

Linear ephemeris: χ^2 = 4099 for 114 d.o.f.	
$T_n = T_0 + Pn$	
T_0 = 2440949.863 ± 0.002 JD	
P = 0.19968775 ± 0.00000007 d	Cov(T_0, P) = -2.3×10^{12}
Parabolic ephemeris: χ^2 = 348.3 for 113 d.o.f.	
$T_n = T_0 + P_0 n + cn^2$	Cov(T_0, P_0) = -2.3×10^{-11} d^2
where $c = P_0\dot{P}/2$	Cov(T_0, c) = 3.5×10^{-16} d^2
T_0 = 2440949.892 ± 0.001 JD	Cov(P_0, c) = -3.8×10^{-20} d^2
P_0 = 0.19968443 ± 0.00000009 d	$\dot{P}$ = (5.76 ± 0.24) $\times 10^{-10}$
c = (5.75 ± 0.16) $\times 10^{-11}$ d	$\dot{P}/P_0$ = (1.05 ± 0.04) $\times 10^{-6}$ yr^{-1}
Cubic ephemeris: χ^2 = 331 for 112 d.o.f.	
$T_n = T_0 + P_0 n + c_0 n^2 + dn^3$	Cov(T_0, P_0) = $(-9.1) \times 10^{-11}$ d^2
where $c_0 = P_0\dot{P}/2$ and	Cov(T_0, c_0) = 3.1×10^{-15} d^2
$d \simeq P_0^2\ddot{P}/6$	Cov(T_0, d) = $(-3.2) \times 10^{-20}$ d^2
T_0 = 2440949.8944 ± 0.0015 JD	Cov(P_0, c_0) = $(-5.5) \times 10^{-19}$ d^2
P_0 = 0.199684009 ± 0.0000003 d	Cov(P_0, d) = 5.9×10^{-24} d^2
c_0 = (7.7 ± 1.1) $\times 10^{-11}$ d	Cov(c_0, d) = $(-2.4) \times 10^{-28}$ d^2
d = (-2.4 ± 1.3) $\times 10^{-16}$ d	$\dot{P}$ = (7.7 ± 1.5) $\times 10^{-10}$
	$\ddot{P}$ = (-1.3 ± 1.6) $\times 10^{-11}$ yr^{-1}
Linear + Sinusoidal ephemeris: χ^2 = 391.1 for 112 d.o.f.	
$T_n = T_0 + P_0 n + c_0 \sin(2\pi(n - \phi)/P_{\rm aps})$	
T_0 = 2440949.92 ± 0.03 JD	
P_0 = 0.199687 ± 9 $\times 10^{-07}$ d	
c_0 = 0.059 ± 0.013 d	
ϕ = 334500 ± 6000 no. of orbit	
$P_{\rm aps}$ = 75.4 ± 0.2 yr	

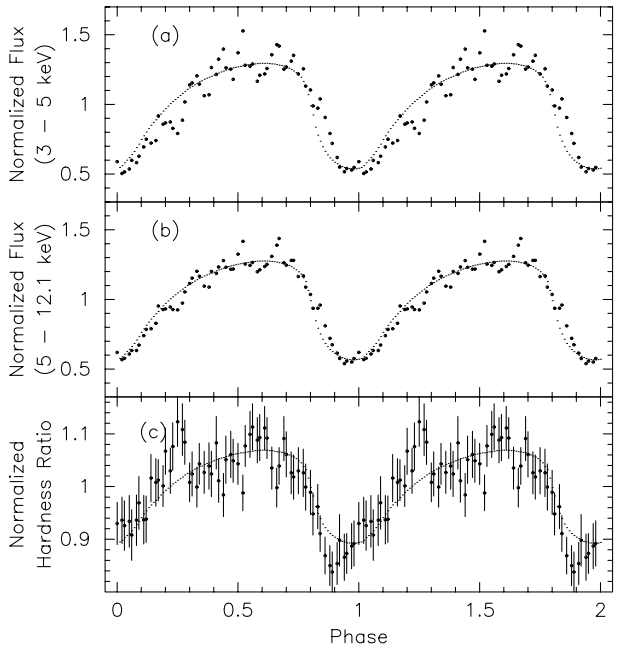

Fig. 4. The folded light curves for Cygnus X-3 with RXTE/ASM in the energy range 3−5 keV and 5−12.1 keV energy ranges along with the normalized template data are shown in panels **a)** and **b)**. The panel **c)** shows the folded hardness ratio of the source plotted on a normalized scale with the template data.

atmosphere. On the other hand, if the companion star is massive, the orbit may widen only if there is significant mass loss from the system in the form of a strong wind and the out-flowing mass carries specific angular momentum of the primary star. The emission line rich X-ray spectrum of Cygnus X−3 detected with Chandra (Paerels et al. 2000) indicates the presence of a strongly photo-ionized stellar wind reminiscent of a high mass companion.

6. Conclusion

- We have measured 34 new minima and extended the measurement base to 30 years.
- The parabolic model provides the best fit to the new data with a modified value of $\dot{P}$.
- A sinusoidal model and the corresponding apsidal motion scenario is ruled out.
- Mass loss from a massive companion is most favoured in Cygnus X−3.

Acknowledgements. We thank the referees for their useful comments and suggestions that improved the contents of the paper. We acknowledge the contributions of the scientific and technical staff of TIFR, ISAC and ISTRAC for the successful fabrication, launch and operation of the IXAE. We thank Dr. S. Seetha and Dr. K. Kasturirangan for their contribution to the IXAE. It is a pleasure to acknowledge the support of Shri K. Thyagarajan, Project Director IRS−P3 satellite, Shri Tyagi, project manager of IRS-P3 and Shri J. D. Rao and his colleagues at ISTRAC. NSS thanks DST, Govt. of India, for providing financial assistance. The work of SN is partially supported by the Kanwal Rekhi Scholarship of the TIFR Endowment Fund.

References

Agrawal, P. C. 1998, in Perspective in High Energy Astronomy and Astrophysics; Proceedings of the International Colloquium, Aug. 12–17, 1996 at TIFR, Mumbai, ed. P. C. Agrawal, & P. R. Viswanath (Universities Press, Hyderabad, India), 408

Batten, A. H. 1973, in Binary and Multiple Systems of Stars, ed. D. Ter Harr (Pergamon Press, Oxford, New York), 86

Bonnet-Bidaud, J. M. & Chardin, G. 1988, PhR, 170, 326

Dickey, J. M. 1983, ApJ, 273, L71

Elsner, R. F., Ghosh, P., Darbo, W., et al. 1980, ApJ, 239, 335

Fender, R. P., Hanson, M. M., & Pooley, G. G. 1999, MNRAS, 308, 473

Ghosh, P., Elsner, R. F., Weisskopf, M. C., & Sutherland, P. G. 1981, ApJ, 251, 230

Hellier, C., Mason, K. O., Smale, A. P., & Kilkenny, D. 1990, MNRAS, 244, 39

Kitamoto, S., Miyamoto, S., Matsui, W., & Inoue, H. 1987, PASJ, 41, 81

Kitamoto, S., Hirano, A., Kawashima, K., et al. 1995, PASJ, 47, 233

Lamb, R. C., Dower, R. G., & Fickle, R. K. 1979, ApJ, 229, L19

Leach, R. W., Murray, S. S., Schreier, E. J., et al. 1975, ApJ, 199, 184

Mason, K. O., Becklin, E. E., Blankenship, L., et al. 1976, ApJ, 207, 78

Mason, K. O., & Sanford, P. W. 1979, MNRAS, 189, 9

Parmar, A. N., Smale, A. P., Verbunt, F., & Corbet, R. H. D. 1991, ApJ, 366, 253

Parmar, A. N., Oosterbroek, T., Del Sordo, S., et al. 2000, A&A, 356, 175

Parsignault, D. R., Schreier, E., Grindlay, J., & Gursky, H. 1976, ApJ, 209, L73

Paerels, F., Cottam, J., Sako, M., et al. 2000, ApJ, 533, L135

Rao, A. R., Agrawal, P. C., Paul, B., et al. 1998, A&A, 330, 181

Schmutz, W., Geballe, T. R., & Schild, H. 1996, A&A, 311, L25

Singh, N. S., Singh, K. Y., Naik, S., et al. 2001, BASI, 29, 351

Tavani, M., Ruderman, M., & Shaham, J. 1989, ApJ, 342, L31

van den Heuvel, E. P. J., & De Loore, C. 1973, A&A, 25, 387

van der Klis, M., & Bonnet-Bidaud, J. M. 1981, A&A, 95, L5

van der Klis, M., & Bonnet-Bidaud, J. M. 1989, A&A, 214, 203

van Kerkwijk, M. H., Charles, P. A., Geballe, T. R., et al. 1992, Nature, 355, 703

White, N. E., & Holt, S. S. 1982, ApJ, 257, 318

Willingale, R., King, A. R., & Pounds, K. A. 1985, MNRAS, 215, 295